

Chapter 5

Mesoscale eddies in the Gulf of Aden

5.1 Introduction

Chapter 4 presented the circulation in the gulf of Aden at the surface and in the deeper layers. It was shown that the currents in the Gulf of Aden are not so simple as thought earlier; they are complicated by the presence of eddies embedded in them. Those eddies influenced the flows in all months. The size of those eddies is comparable to the width of the gulf ($\sim 250\text{--}300$ km) (Figure 4.3). They often extend to the deeper layers; at least up to 1000 m (Figure 4.5). Earlier Bower et al. [2002, 2005] described the presence of cyclonic and anticyclonic eddies in the gulf at intermediate depths ($\sim 100\text{--}600$ m) and discussed their role in spreading the Red Sea Water in the gulf. They noted that the azimuthal speed of advecting eddies was as high as $20\text{--}30$ cm s⁻¹. Based on the water properties in the centre of an anticyclonic eddy, Bower et al. [2002] argued that they are first formed in the Somali Current system and then transported into the gulf. Some of the earlier studies also noted the presence of the eddies in the Gulf of Aden, but did not describe their origin or resident time in the gulf [Piechura and Sobaih, 1986; Nasser, 1992; Awad and Kolli, 1992; Johns et al., 2001]. Recently, Fratantoni et al. [2006] described a series of eddies entering the gulf mostly during the transition between the

summer and winter monsoons. The cyclonic and anticyclonic eddies of approximately 250 km diameter translated towards the west at speeds of 5–8 cm s⁻¹. These eddies entering the gulf from the Arabian Sea are different from the large eddies (the Great Whirl, Southern Gyre, etc.) that develop in the western boundary region during the northern summer (see Schott and McCreary [2001] for a detailed discussion).

Except for Simmons et al. [1988] and Fratantoni et al. [2006], no other study has examined the characteristics of these eddies or their origin. Simmons et al. [1988] related the eddies near the Gulf of Aden to the break up of the upwelling band in late July and early August and the flow from the Great Whirl through the Socotra passage. Fratantoni et al. [2006] argued that a portion of the Somali Current that accelerates northward through the Socotra Passage retroflects sharply and collapses to form discrete anticyclonic current rings, which move westward into the gulf. In particular, they used this mechanism to explain the eddies entering the gulf during the fall inter-monsoon. Similarly, the variability in the Socotra Passage flow was also argued to be the cause of the generation of rings in May during the transition between the winter and summer monsoons. Fratantoni et al. [2006] did not, however, explain the other eddies seen from altimeter derived geostrophic currents; in particular, they did not propose a mechanism for the eddies that moved into the gulf from the interior of the Arabian Sea. Our analysis in Chapter 4 showed that the eddies exist in the Gulf of Aden round the year. In this chapter¹, we describe the characters of these eddies in detail and investigate the possible reasons for eddy formation in the vicinity of the gulf and their westward movement.

¹This chapter is based on the paper by **Al Saafani, M. A.**, S. S. C. Shenoi, D. Shankar, M. Aparna, J. Kurian, F. Durand, and P. Vinayachandran. Westward movement of eddies into the Gulf of Aden from the Arabian Sea. *J. Geophys. Res.*, 112, C11004, doi:10.1029/2006JC004020, 2007.

5.2 Westward movement of eddies in the gulf

The data used for this analysis are the 11 years (1993-2003) weekly altimeter derived SLA described in Chapter 2.

Figure 5.1 shows the evolution of SLA from June 1999 to April 2000, highlighting the occurrence of cyclonic/anticyclonic eddies in the western Arabian Sea. We chose 1999–2000 as a typical year to demonstrate the westward propagation of eddies in the gulf particularly, during winter. Other years too showed similar westward propagating eddies (see Figure 5.2). Westward movement, however, was not apparent during the summer monsoon, though some eddies were seen in the region in June. During 1999–2000, the anticyclonic eddy seen at 14° N, 53° E on 2 June moved slightly eastward to 14° N, 54° E on 16 June. By 30 June, it had weakened considerably; it disappeared on 28 July. Simultaneously, the large patch of high sea level (SL) seen inside the gulf weakened, broke into two smaller patches (on 30 June), and shrank gradually (in the second half of July), paving the way for a large patch of low SL on 25 August. The large patch of low SL in the gulf continued through September and October and an anticyclonic eddy formed to the east of the gulf at 54° E during the end of the summer monsoon (see the panel for 22 September). This eddy moved westward to 52° E on 20 October, reached the entrance of the gulf at 51° E on 3 November, and moved westward in the gulf during December-1999–January-2000. It arrived at 48° E on 26 January, reached the western end of the gulf on 22 March, and dissipated thereafter. The entry of this anticyclonic eddy into the gulf in December pushed the existing low SL in the gulf towards the west, and the latter manifested as a cyclonic eddy in the western gulf. During February 2000, another anticyclonic eddy manifested at 58° E and propagated into the gulf during March–April. An extended version of Figure 5.1 depicting the evolution of SLA for all the years during 1993 to 2003 is available as an animation at <http://www.agu.org/journals/jc/jc0711/2006JC004020/>.

The trajectories of eddies shown in Figure 5.2 confirms the westward propagation during all the 11 winters analyzed here, though the tracks of these eddies (cyclonic/anticyclonic)

Figure 5.1 Sequence of altimeter-derived SLA (cm) maps during June 1999 to April 2000, highlighting the presence of cyclonic/anticyclonic eddies inside and outside the Gulf of Aden. The SLA data are from the merged TOPEX/Poseidon and ERS-1/2 data set. The broken contours indicate negative SLA.

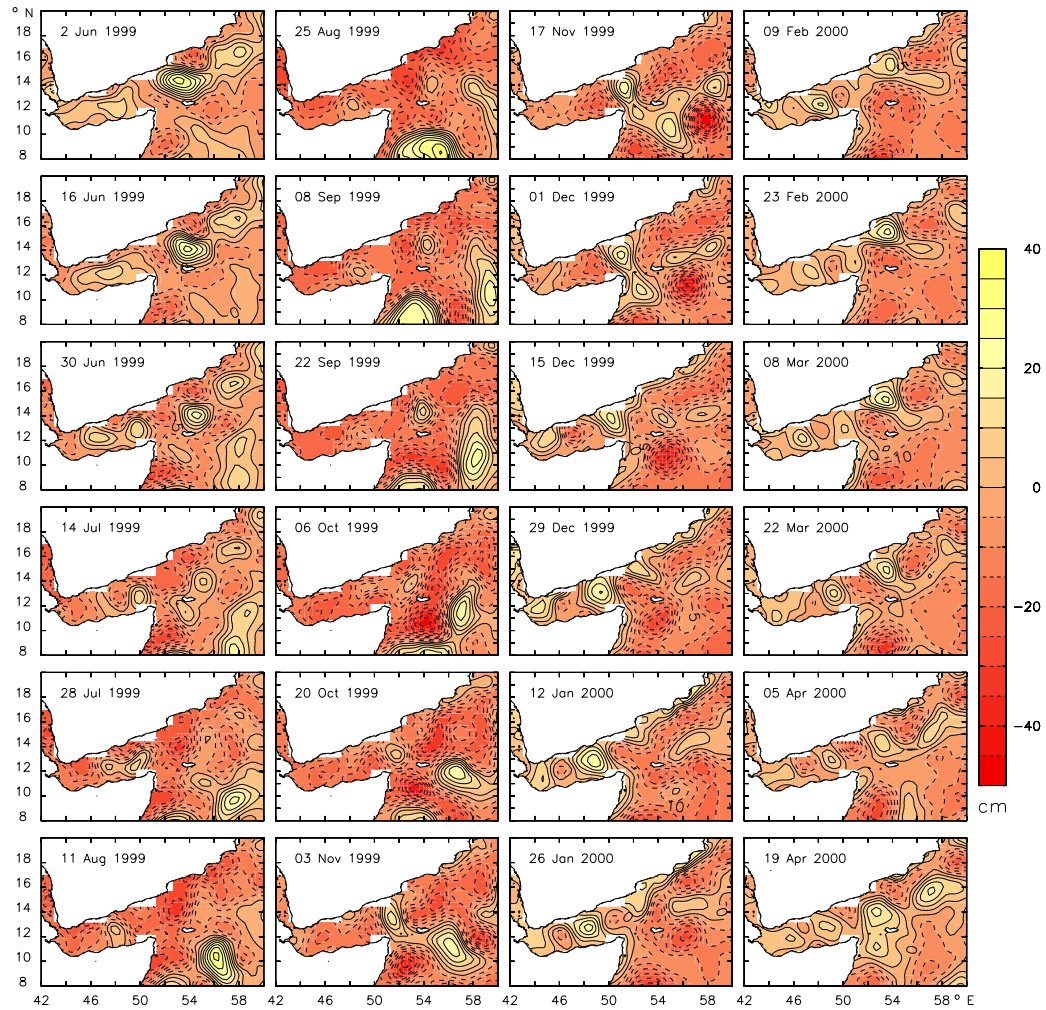
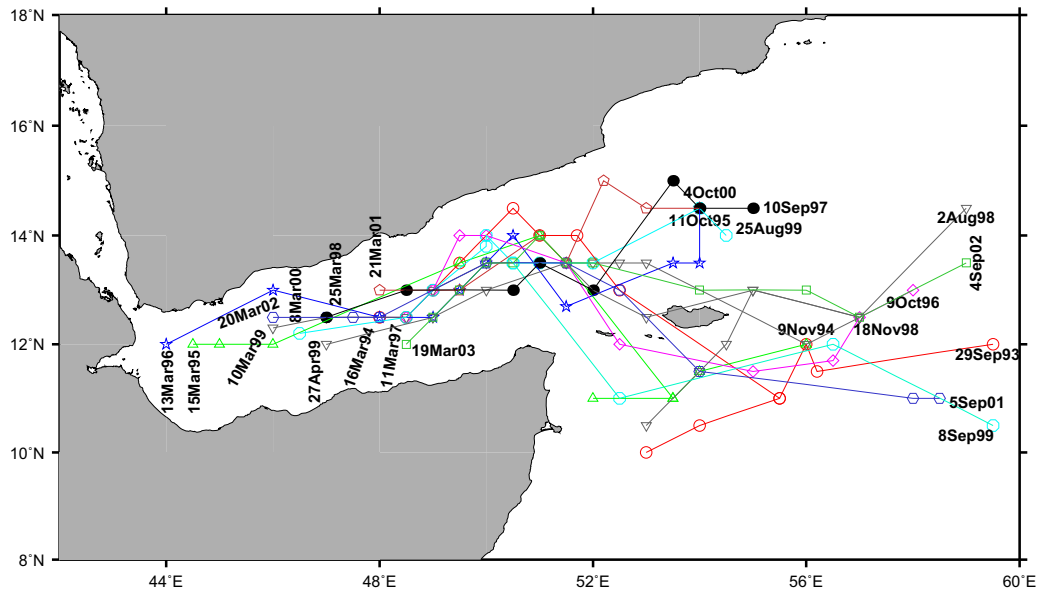


Figure 5.2 The trajectories of eddies entering the Gulf of Aden during 1993–2003. The locations of eddies were derived from the merged TOPEX/Poseidon and ERS-1/2 altimeter SLA data set.



did vary from year to year. Westward propagation was apparent in the SLA maps during winter, but it was absent/weak during the summer monsoon, especially during August–September. During the winter monsoon, the anticyclonic eddies arriving near the Socotra Island from the east propagated directly into the gulf (1995–1996, 1997–1998, 1998–1999, 1999–2000 and 2000–2001) or propagated into the gulf after passing through the Socotra passage (1993–1994, 1994–1995, 1996–1997, 2001–2002, and 2002–2003). In some cases (1997–1998, 1998–1999, and 2002–2003) the eddy that arrived from the east, split into two at Socotra Island before propagating into the gulf; the upper portion propagated directly into the gulf, while the lower portion propagated into the gulf after passing through the Socotra passage. This is seen clearly in the animation available at <http://www.agu.org/journals/jc/jc0711/2006JC004020/>. Once they entered the gulf, the eddies usually propagated till 46° E and decayed thereafter during March–May. Some eddies, though very few, continued to the western end of the gulf at 44° E (Figure 5.2).

To estimate the westward propagation speed inside the gulf, a Hovmöller diagram (longitude vs time) of SLA was constructed for the gulf (43° E to 51° E) (Figure 5.3). During the summer monsoon, westward propagation was weak and not discernible except during the summers of 1997, 2000, and 2001. From the slope of the propagating anomalies (Figure 5.3), the propagation speed was estimated to be 6.0–8.5 cm s⁻¹. The maximum azimuthal velocities of the eddies estimated from the geostrophic balance was 50–70 cm s⁻¹. These values are similar to those reported by Fratantoni et al. [2006].

5.3 Mechanisms

We saw that the eddies first appeared outside the gulf in the Arabian Sea and propagated westward to enter the gulf mostly during early winter. This movement continued till March and for some years till May. During summer, no clear westward propagating eddies were discernible in the gulf because of the large patch of low SL that covered the region (Figure 4.3 and 5.1). In the following subsections, we analyse the three basic mechanisms that can cause or favour the generation of westward moving mesoscale eddies in the Gulf of Aden.

5.3.1 Local Ekman pumping

The spatial variation in the wind stress on the sea, i.e., a non-vanishing curl of wind stress, could cause a divergence of the surface layer causing upwelling (positive Ekman pumping) or convergence of the surface layer causing downwelling (negative Ekman pumping). Localised regions of Ekman pumping can then force eddy motions in the ocean. To check whether the eddies and the large patch of low SL were forced by the local wind-stress curl, we have estimated the Ekman pumping velocity (W_e) at the entrance of the gulf following Smith [1968] as follows

Figure 5.3 Time-longitude plot (Hovmoller diagram) of SLA along 12.5° N in the Gulf of Aden (43° E to 51° E). Zero SLA values are contoured.

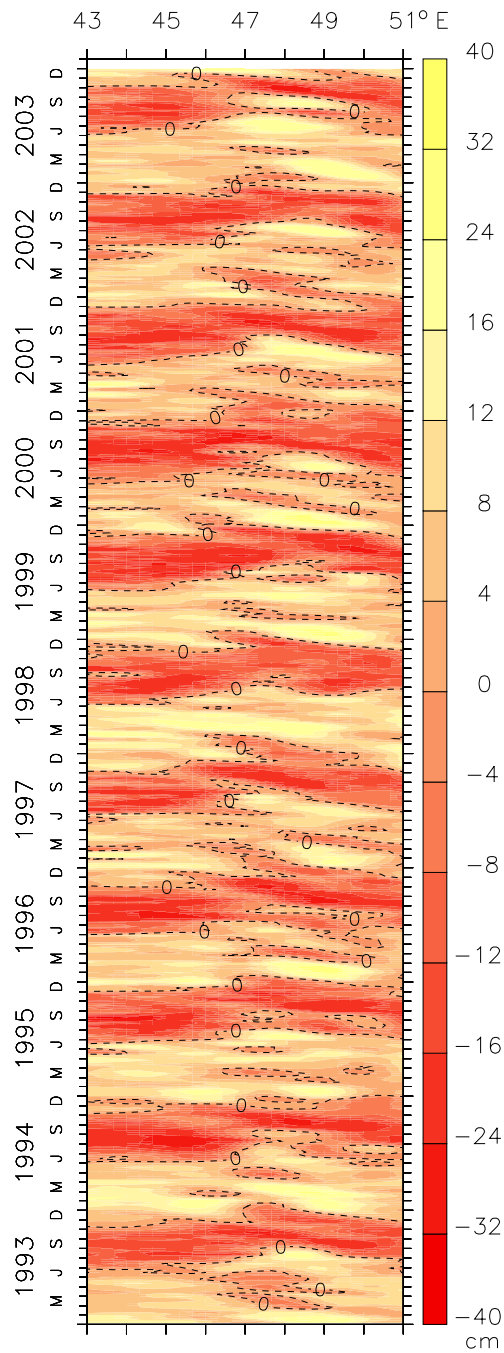
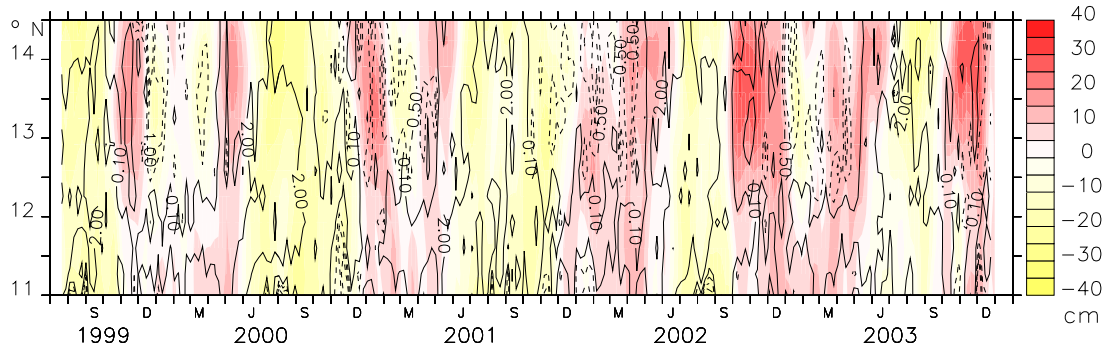


Figure 5.4 Time-latitude plot of SLA and Ekman pumping velocities at the entrance of the Gulf of Aden (along 51.5° E) between the latitudes 11° N and 14.5° N. The shading is for SLA (cm) and the overlaid contours are for Ekman pumping velocities (m day^{-1}); contour interval is 0.5 m day^{-1} . Negative values of Ekman pumping velocities are represented by broken contours.



$$W_e = \frac{1}{\rho} \text{curl} \left(\frac{\tau}{f} \right) = \frac{1}{\rho} \left[\frac{\text{curl}(\tau)}{f} + \frac{\tau_x \beta}{f^2} \right] \quad (5.1)$$

where τ is the wind stress, τ_x is the x-component of τ , β is the rate of change of Coriolis parameter (f) with latitude and ρ is the density of sea water.

QuikSCAT wind data (described in Chapter 2) were used to estimate W_e (Figure 5.4). The comparatively strong (2 m day^{-1}) positive W_e was in phase with the negative SLA during June–September for all years (1999–2003) (Figure 5.4). On the contrary, the weak W_e ($\sim 0.5 \text{ m day}^{-1}$) was out of phase with the cyclonic/anticyclonic eddies during November–May: for example, during 1999, W_e was positive (negative) when the anticyclonic (cyclonic) eddy appeared in November (December), and it was negative (positive) when the cyclonic (anticyclonic) eddy appeared in March–April (April–May) 2000 (Figure 5.4). Hence, local Ekman pumping cannot be the cause of the eddies entering the gulf during winter, but it can force the low SL during summer.

5.3.2 Westward propagating Rossby waves in the Arabian Sea

The northern Indian Ocean, specially the Arabian Sea adjacent to the Gulf of Aden is known for the westward propagating Rossby waves [McCreary et al., 1993; Shankar and Shetye, 1997]. In the Arabian Sea, the westward propagating Rossby waves were produced either by radiation from the west coast of India in association with poleward propagating coastal Kelvin waves [McCreary et al., 1993; Shankar and Shetye, 1997], or by the forcing due to Ekman pumping over the Arabian Sea (see, for example, [McCreary et al., 1993; Prasad and Ikeda, 2001; Brandt et al., 2002; Shankar et al., 2002]). The Rossby waves or planetary waves arise from the need to conserve the potential vorticity. Rossby waves have been difficult to detect in the oceans because of their small sea surface signature (height variation of order of 10 cm or smaller), slow propagation speeds (of order of 10 cm s^{-1} or less), and long wavelengths (hundreds to thousand km). The advent of satellite altimetry opened a new era for detection of these Rossby waves [Chelton and Schlax, 1996]. Hence, the satellite derived SLA in the Arabian Sea was analysed to understand the propagation of Rossby waves and the associated alternating patches of high/low sea levels or anticyclonic/cyclonic eddies.

A Hovmoller diagram of altimeter derived SLA for the Arabian Sea at 12.5° N (which passes through the center of the gulf) shows the westward propagating highs and lows in the SLA (Figure 5.5a), associated with the westward propagating Rossby waves. The propagations extended from the coast of India (75° E) to the western gulf (47° E). The annual cycle of westward propagating SLA was outstanding, but other periodicities were also evident. The slope of alternating highs and lows was uniform between 75° E and 50° E , but changed abruptly to the west of 50° E . The westward propagating signal took about 250–270 days to travel from the coast of India (75° E) to the gulf (50° E) (Figure 5.5), which implies a speed of $\sim 11.7\text{--}12.7 \text{ cm s}^{-1}$.

To check whether these speeds match with the theoretical speeds of the westward propagating Rossby waves, we have estimated the phase speeds of the first and second

mode annual baroclinic Rossby waves, by solving an eigenvalue problem that depends only on the local stratification [LeBlond and Mysak, 1978]. The Brunt-Vaisala frequency (stability frequency) ($N^2 = \frac{g}{\bar{\rho}} \frac{\partial \rho}{\partial z}$) profiles used for the vertical mode expansions were estimated from temperature [Stephens et al., 2002] and salinity [Boyer et al., 2002] climatologies for the Arabian Sea, g is the acceleration due to gravity, $\bar{\rho}$ is the mean density of seawater in the water column and ρ is the density of seawater at each depth level.

We followed Shankar et al. [1996] to solve the eigenvalue problem to obtain the phase speed of first and second modes. These modes are the eigenfunctions, $\psi_n(0)$, that satisfy

$$\frac{\partial}{\partial z} \left(\frac{1}{N^2} \frac{\partial \psi_n}{\partial z} \right) = \frac{-1}{c_n^2} \psi_n(z) \quad (5.2)$$

subject to boundary condition

$$\frac{\partial \psi_n}{\partial z}(-D) = \frac{\partial \psi_n}{\partial z}(0) = 0 \quad (5.3)$$

They form an orthogonal set; they are normalized so that

$$\psi_n(0) = 1 \quad (5.4)$$

and are ordered so that their eigenvalue (characteristic speed) c_n decreases monotonically with n . The $n = 0$ eigenfunction is the barotropic mode of the system. The eigenfunctions for $n \geq 1$ are the baroclinic modes, and their eigenvalues are finite. Equations 5.2, 5.3 and 5.4 then imply that $\int_{-D}^0 \psi_n dz = 0$ for $n \geq 1$ so that horizontal transport relative to the ocean bottom associated with each baroclinic mode vanishes. The phase speed of each mode, c_{rn} were then obtained from the eigenvalues, c_n as

$$c_{rn} = \beta \frac{c_n^2}{f^2} \quad (5.5)$$

At 12.5° N the phase speed of first (c_{r1}) and second (c_{r2}) baroclinic modes work out to be 12.7 cm s^{-1} and 4.1 cm s^{-1} respectively. The estimated theoretical speed of the first-mode Rossby wave is comparable to the speed of westward propagation of SLAs

in Figure 5.5, suggesting that the eddies entering the gulf from the east are associated with westward propagating Rossby waves in the Arabian Sea. The theoretical estimate of the phase speeds of first and second mode Rossby waves are in good agreement with the earlier estimates of Brandt et al. [2002]. They estimated the speeds of first and second mode baroclinic annual Rossby waves at 8° N as 38.0 cm s^{-1} and 14.0 cm s^{-1} ; they used the hydrographic data acquired during August 1993. Our estimates for the same modes at 8° N are 31.35 cm s^{-1} and 11.25 cm s^{-1} .

A similar analysis using the average Brunt-Vaisala frequency profile in the gulf yielded a lower Rossby wave phase speed for the first mode owing to a shallower thermocline: the thermocline inside the gulf is $\sim 20\text{--}50$ m shallower than that in the Arabian Sea at 12.5° N latitude (Figure 5.6). The theoretical speed of 7.2 cm s^{-1} is comparable to the SLA propagation speed of $\sim 6.0\text{--}8.5 \text{ cm s}^{-1}$ inside the gulf (Figure 5.3). This decrease in Rossby wave phase speed causes the abrupt change of slope at 50° E in the SLA Hovmoller diagram (Figure 5.5a).

In most of the years, the westward propagating signal was amplified at around $52\text{--}60^\circ$ E. The propagations also showed a discontinuity at this location. The discontinuities were sharp during 1996 and 1998–2001 (Figure 5.5a). To check if this discontinuity occurred at all frequencies, the SLA was partitioned using a low-pass filter (180-days or 26-weeks running mean). The Hovmoller diagram for the low-frequency (high-frequency) part is shown in Figure 5.5b (Figure 5.5c). The Hovmoller diagrams clearly show that both high- and low-frequency Rossby waves propagated from the west coast of India towards the gulf. The high-frequency waves were amplified between 52° E and 60° E while propagating westward (Figure 5.5c). The amplification in this longitude band started around 60° E in September or in early October. No such amplification was apparent in the low-frequency band as the waves propagated westward (Figure 5.5b), but discontinuities were seen in this longitude band at the low frequencies. Hence, we conclude that the amplification seen in Figure 5.5a between 52° E and 60° E was due to high-frequency

waves and the discontinuity was due to low–frequency waves. Both low– and high–frequency waves propagated westward all across the Arabian Sea. Analysis along other latitudes (8 and 10° N) also showed the amplifications and discontinuities west of 60° E (Figure 5.7).

We have seen that there is an abrupt change in Rossby wave speed across the mouth of the gulf owing to a change in thermocline depth (Figure 5.6). The phase speeds estimated above were based on an average stratification for the Arabian Sea and the gulf (at 12.5° N). The thermocline depth, and therefore stratification, in the Arabian Sea changes in both space and time owing to time–dependent monsoonal circulation (see Schott and McCreary [2001]). Hence, to check the role of varying background stratification in modifying the propagation speeds, the phase speeds of first and second baroclinic mode annual Rossby waves along 12.5° N for each month (Figure 5.8) were estimated. The phase speed of the first mode (Figure 5.8a) peaked near 60° E during summer and near the west coast of India during winter (Figure 5.8a). The phase speed of the second mode also peaked between 55–62° E during summer (Figure 5.8b) and near the west coast of India during winter. The summer peak in the western Arabian Sea coincided with the deepest thermocline in the region (~ 180 m; Figure 5.8c) and the winter peak near the west coast of India with downwelling Rossby waves.

Thus, the stratification and Rossby wave speeds varied considerably in both time and space along 12.5° N in the Arabian Sea. Hence, to check whether the propagating signals, evident at both low and high frequencies in the SLA, are significant, we performed a wavelet analysis on weekly SLA for 11 years along 12.5° N from the west coast of India to the Gulf of Aden (Figure 5.9a). The annual signal was dominant and significant (at 95% confidence level) at all locations from the west coast of India to Gulf of Aden for all years except during 2001–2003 at 55° E.

The high–frequency signals (period less than 180 days) seen in the Hovmoller diagrams (Figure 5.5a and c) were not significant (at 95% confidence level) east of 61° E,

but were significant in the west (Figure 5.9a). The significant high frequencies included oscillations starting from about 60–80 days, but the most notable frequencies were in the 90–180 days band. The wavelets confirmed the concentration of energy in the high-frequency band seen between 52° E and 58° E in the Hovmoller diagram (Figure 5.5c). In general, the wavelet power spectrum was patchy and the high-frequency wavelets were significant only west of 60° E during September–October, but there was considerable interannual variability: at 55° E, the wavelets were significant in the band around ~ 100 –200 days between September 1995 and March 1999 and again between September 2001 and August 2003. The wavelet analysis also showed significant sub-annual signals; an analysis of these frequencies is, however, beyond the scope of this study.

A similar analysis on Ekman pumping, estimated from QuikSCAT winds for 1999–2003, was also performed to check the contribution of local winds to the Rossby waves at 12.5° N. The annual frequency was not significant (at the 90% confidence level) in the east, but was significant west of 60° E (Figure 5.9b). At most locations, the wavelets of Ekman pumping in the high-frequency band (~ 15 days to ~ 160 days) were significant, but only during the summer monsoon (May–September). Like the high-frequency wavelets of SLA, the high-frequency wavelets of Ekman pumping (~ 100 –160 days) were also most prominent between 52 – 58° E; the maximum wavelet power was seen at 55° E during 2001–2003, coinciding with the period and location of maximum high-frequency wavelet power in the SLA (Figure 5.9a). From the wavelets of SLA and Ekman pumping, it is clear that the local winds play an insignificant role in generating annual Rossby waves east of 60° E, but they do play a significant role in modulating the waves west of 60° E. The local winds also generate high-frequency Rossby waves in the longitude band 52 – 58° E. This lack of Rossby wave generation by Ekman pumping east of 60° E implies that the Rossby waves radiating from the eastern boundary (Figure 5.5) are generated by (the mostly remotely forced) coastal Kelvin waves along the Indian west coast [McCreary et al., 1993; Shankar and Shetye, 1997; Nethery and Shankar, 2007]. The wavelet analysis

Figure 5.5 Time–longitude plots (Hovmoller diagram) of (a) observed SLA (cm), (b) the low-frequency (> 180 days) part of SLA (cm), and (c) the high-frequency (< 180 days) part of SLA (cm) along 12.5° N in the Arabian Sea. The 12.5° N latitude was selected because it passes through the center of the Gulf of Aden. Zero SLA values are contoured.

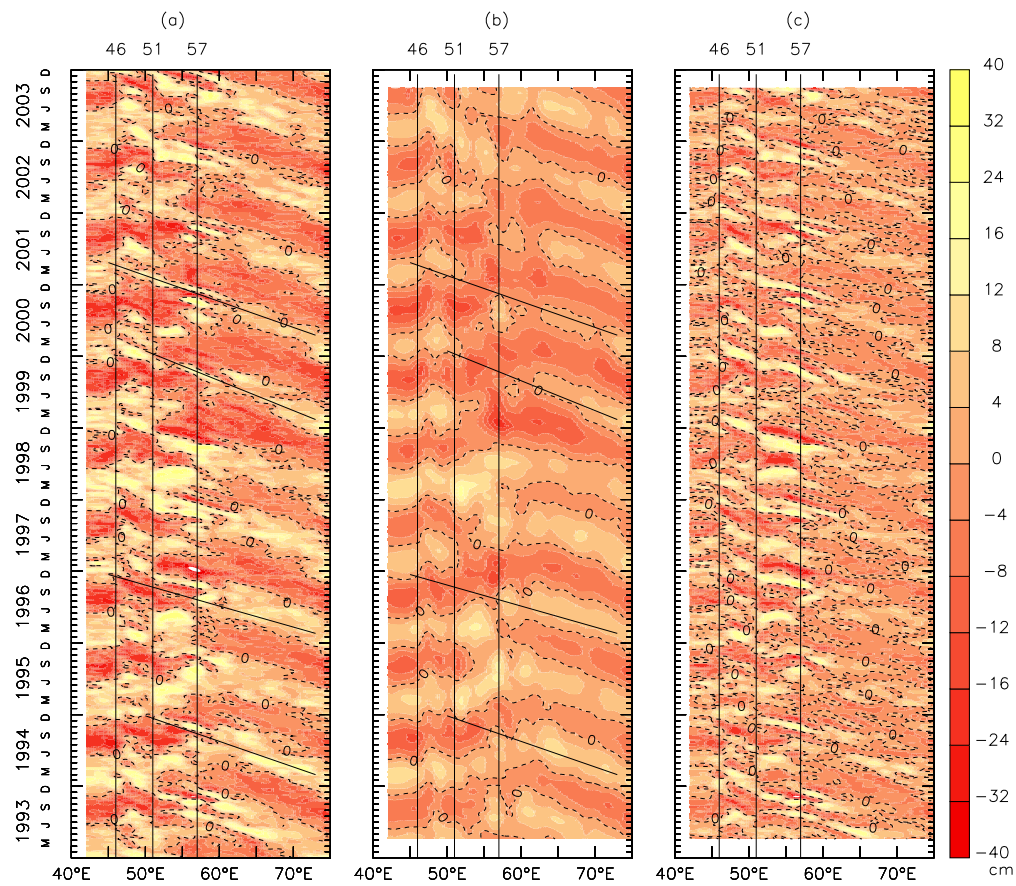
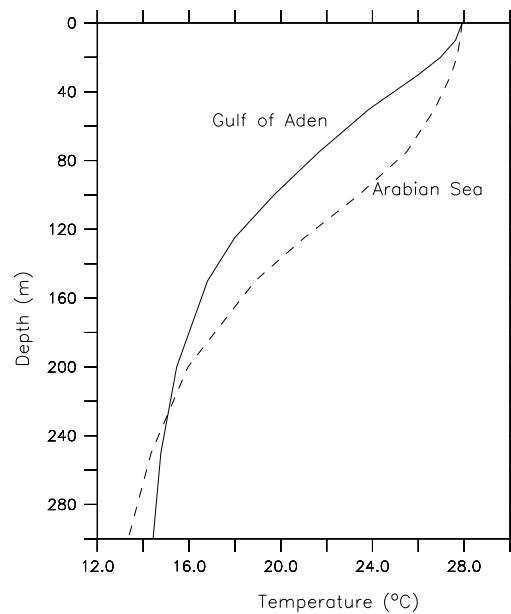


Figure 5.6 Mean temperature profile ($^{\circ}\text{C}$), estimated from Stephens et al. [2002] along 12.5°N inside the Gulf of Aden (43°E to 51°E) and the Arabian Sea (55°E to 75°E).



also suggests considerable interannual variability in the local generation of Rossby waves at both low and high frequencies.

5.3.3 Instabilities in western boundary currents

The other sources of cyclonic and anticyclonic eddies that enter the Gulf of Aden are the eddies generated when a part of the Somali current accelerates northward through the Socotra passage [Fratantoni et al., 2006]. Simmons et al. [1988] had noted that when the Findlater Jet, a strong low level jet in the atmosphere associated with the monsoon system over the Arabian Sea [Findlater, 1969], and its associated curl field begin to relax in late July and early August, a broad upwelling band begins to break up into several large eddies in the vicinity of the Gulf of Aden (see their Plate 1). The Great Whirl impinges on the Socotra Island, and the associated flow through the Socotra passage strengthens and continues northward to the Yemen coast, where it turns to the east to flow as a large

Figure 5.7 Time-longitude (Hovmöller diagram) of observed SLA (cm) along (a) 8° N and 10° N latitudes. Zero SLA values are contoured.

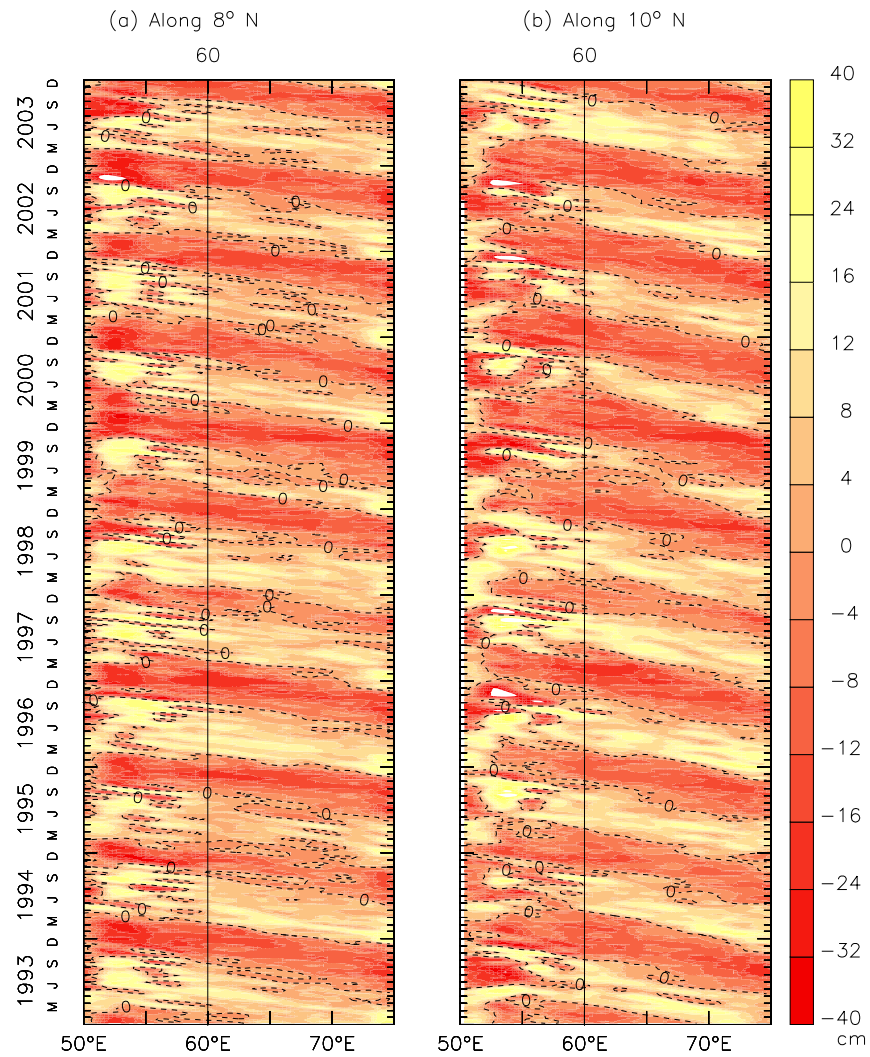


Figure 5.8 Time–longitudes plots (Hovmoller diagram) of (a) the phase speed of the first mode baroclinic Rossby wave (cm s^{-1}), (b) the phase speed of the second mode baroclinic Rossby wave (cm s^{-1}), and (c) the depth of 18°C isotherm (indicative of the depth of the thermocline) estimated from [Stephens et al., 2002] along 12.5°N in the Arabian Sea. The two horizontal lines are drawn for January (winter monsoon) and September (summer monsoon), for which a section through this contour plot is shown in (d). The location of Socotra Island is hatched.

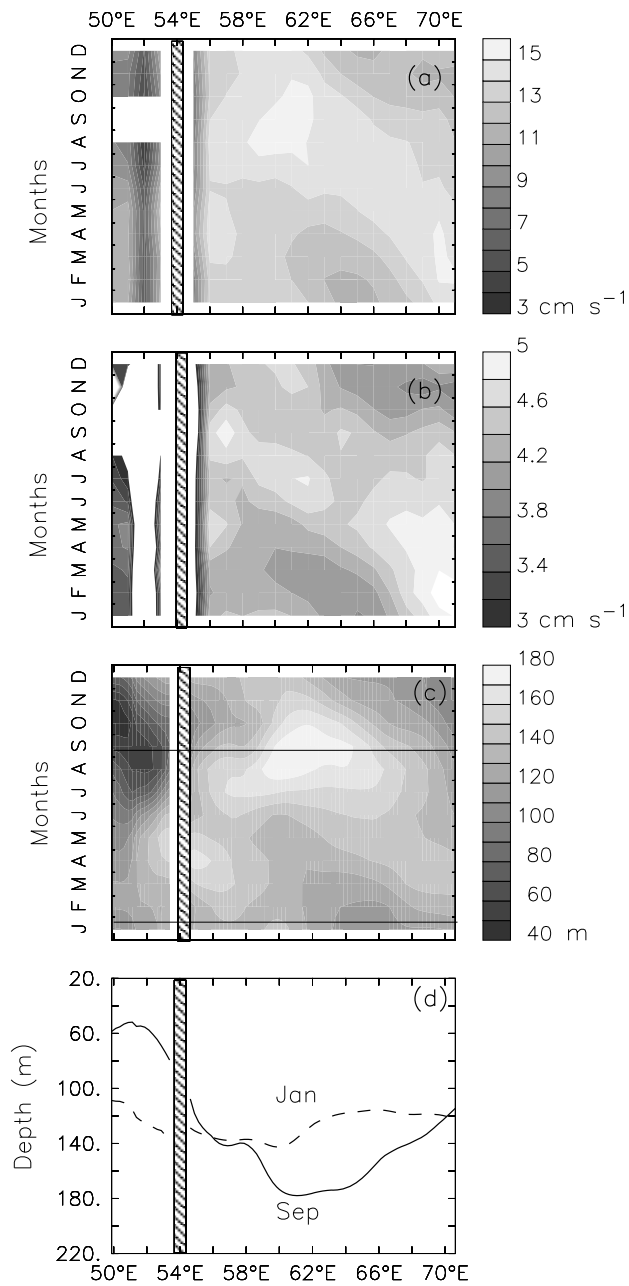


Figure 5.9 (a) Time–scale representation of the wavelet power spectrum of the SLA time series along 12.5° N.

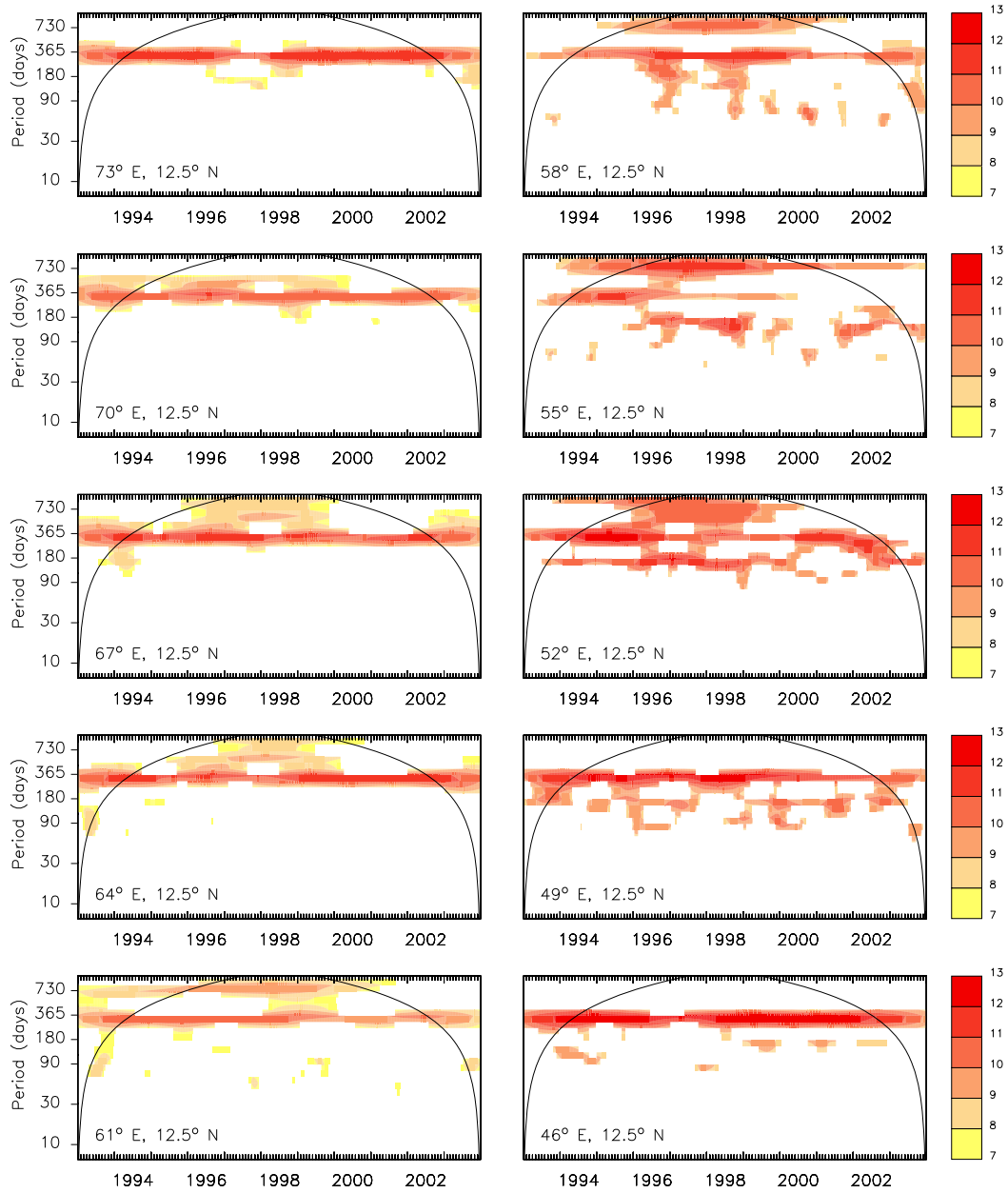
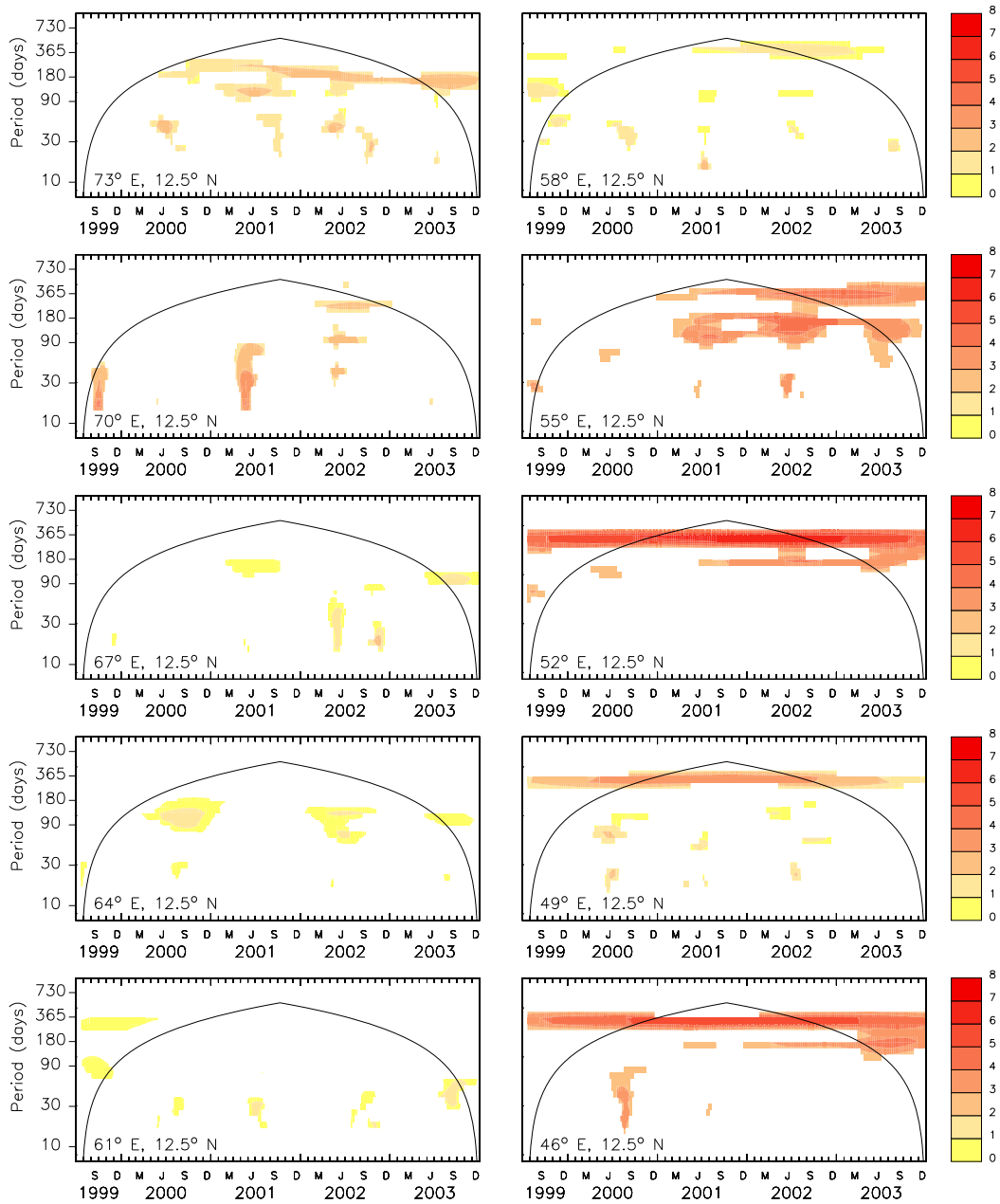


Figure 5.9 (b) Same as 5.9a for Ekman pumping estimated from the QuikSCAT winds for the period 1999 to 2003.



meander. Later in mid-September, the outflow from the Great Whirl causes the formation of Socotra Gyre [Simmons et al., 1988]. This mechanism, in which eddies pinch off from the Somali Current system owing to instabilities, is also active during May [Fratantoni et al., 2006].

To examine the type of instabilities that occur in the flow across the mouth of the gulf, we analysed the energy cycle. The results of an ocean general circulation model (MOM4) simulation for the Indian Ocean [Kurian and Vinayachandran, 2006, 2007] were used to compute the mean and eddy components of energy. The model had a horizontal resolution of $0.25^\circ \times 0.25^\circ$ and had 40 levels in the vertical, with 5-m resolution in the upper 60 m. The model was forced by daily climatology derived from the European Centre for Medium-Range Weather Forecasts (ECMWF) reanalysis (ERA-15) for 1979–1993 [Roske, 2001]. The model, an extensive validation of which was presented by Kurian and Vinayachandran [2007], reproduced (Figure 5.10) the eddies and the westward propagation seen in the observed SLA outside the gulf. Figure 5.10a shows westward propagation of the signal along 12.5° N similar to that seen from altimeter derived SLA (Figure 5.10b). Inside the gulf, however, the model was unable to simulate all the observed features: for example, the model westward propagation was weak during January–May. This limitation of the model, however, should not affect the instability analysis presented here because the analysis was carried out for a box outside the gulf.

Energy budget is presented in the form of a box diagram introduced by Lorenz [1955] showing the energy transfer terms acting upon the various components of the total energy. The mean kinetic energy (MKE), eddy kinetic energy (EKE), mean available potential energy (MPE), eddy potential energy (EPE), and the transfer terms between the energy components were estimated following the formulation used by Boning and Budich [1992]; Vinayachandran and Yamagata [1998] as follows.

The available potential energy per unit mass in a volume element V can be approximated as

$$P = -\frac{1}{2}g \int \int \int \frac{(\rho - \tilde{\rho})^2}{d\tilde{\rho}/dz} dV \quad (5.6)$$

or, using the linear relation between potential density and potential temperature, $\rho = \rho_0(1 - \alpha T)$, where $\alpha = 2.5 \times 10^{-4}$, the relation is rewritten as

$$P = \frac{1}{2}\alpha g \int \int \int \frac{(T - \tilde{T})^2}{d\tilde{T}/dz} dV \quad (5.7)$$

The reference state, $\tilde{T}(z)$, is obtained from the horizontal average over the time-mean temperature distribution. Neglecting the contribution of vertical velocity w , the kinetic energy per unit mass is given by

$$K = \frac{1}{2} \int \int \int (u^2 + v^2) dV \quad (5.8)$$

Separating the actual flow variables into time mean and transient parts, $u = \bar{u} + u'$, $v = \bar{v} + v'$, etc., the time-mean energy of the system may be divided into four components: mean available potential energy

$$MPE = \frac{1}{2}\alpha g \int \int \int \frac{(\bar{T} - \tilde{T})^2}{d\tilde{T}/dz} dV, \quad (5.9)$$

eddy available potential energy

$$EPE = \frac{1}{2}\alpha g \int \int \int \frac{\overline{T'^2}}{d\tilde{T}/dz} dV, \quad (5.10)$$

mean kinetic energy

$$MKE = \frac{1}{2} \int \int \int (\bar{u}^2 + \bar{v}^2) dV, \quad (5.11)$$

eddy kinetic energy

$$EKE = \frac{1}{2} \int \int \int (\overline{u'^2 + v'^2}) dV, \quad (5.12)$$

When integrated over a closed domain, the energy component changes by the work of external forces on the system, that is, wind work (W) and buoyancy work (B), by diffusion (D) and frictional dissipation (F), or by the transfer of energy due to interactions with other components.

Thus the energy transfer (Tr_i), per unit mass, in a closed volume V is given as

$$Tr_1 = \alpha g \int \int \int \overline{wT} dV \quad (5.13)$$

$$Tr_2 = \alpha g \int \int \int \frac{\overline{u'T'}\partial\overline{T}/\partial x + \overline{v'T'}\partial\overline{T}/\partial y}{d\overline{T}/dz} dV \quad (5.14)$$

$$Tr_3 = -\alpha g \int \int \int \overline{w'T'} dV \quad (5.15)$$

$$Tr_4 = - \int \int \int \left\{ \overline{u'u'} \frac{\partial \overline{u}}{\partial x} + \overline{u'v'} \left(\frac{\partial \overline{v}}{\partial x} + \frac{\partial \overline{u}}{\partial y} \right) + \overline{v'v'} \frac{\partial \overline{v}}{\partial y} \right\} dV \quad (5.16)$$

where Tr_1 represents the conversion of mean kinetic to mean potential energy by the work of mean buoyancy force, Tr_2 the conversion of mean to eddy potential energy (baroclinic instability), Tr_3 the conversion from eddy potential to eddy kinetic energy, and Tr_4 the work of the Reynolds stresses against the mean shear (which, if positive, represents barotropic instability).

Complete energy analysis is not attempted because it is beyond the scope of this work. The mean and eddy components were calculated from the daily snapshots of the seventh year of the simulation [Kurian and Vinayachandran, 2006, 2007]. The energy components and their transfer terms (Figure 5.11) were estimated separately for the top 200 m for three periods representing the summer monsoon (June–September), the winter monsoon (November–February), and the transition period between the monsoons (March–May). During the winter monsoon and the transition period, energy was directly transferred from MKE to EKE, implying that the barotropic instabilities were responsible for the generation of the eddy that appears near the gulf. During the summer monsoon, however, energy was transferred not only from MKE to EKE, but also from MPE to EPE and from MKE to MPE, implying that the transfer from the pool of kinetic energy maintained the mean potential energy against the work of the buoyancy forces and that the eddies were generated owing to both barotropic and baroclinic instabilities.

Figure 5.10 Time–longitude plots (Hovmoller diagram) of (a) SLA along 12.5° N from MOM4 Kurian and Vinayachandran [2006, 2007] and (b) altimeter derived SLA along the same latitude.

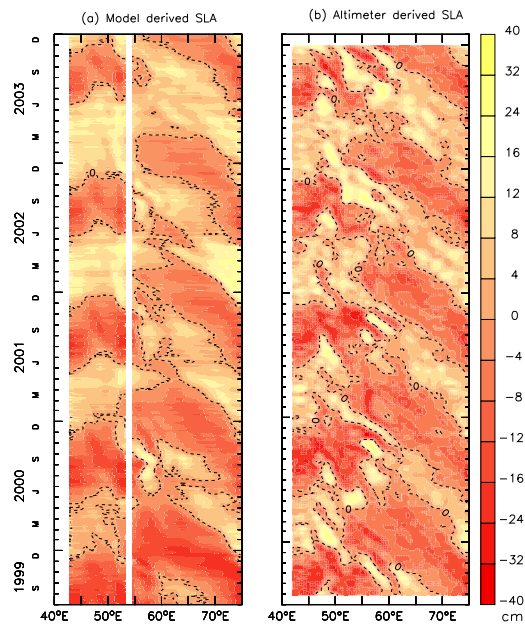
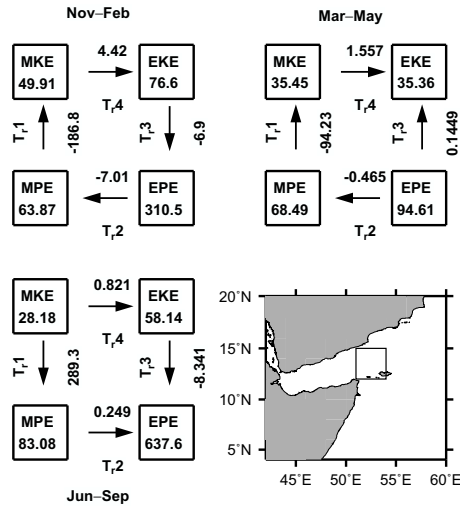


Figure 5.11 Values of the energy components ($\text{cm}^2 \text{s}^{-2}$) and transfer terms ($10^{-5} \text{cm}^2 \text{s}^{-3}$) for a $3^\circ \times 3^\circ$ box outside the gulf ($12\text{--}15^\circ \text{N}$, $51\text{--}54^\circ \text{E}$; see inset). A 200-m deep water column was considered for the computation of energy components and transfer terms using the OGCM results of Kurian and Vinayachandran [2006] and Kurian and Vinayachandran [2007]



5.4 Discussion

5.4.1 Westward moving eddies in the Gulf of Aden and westward propagating Rossby waves in the Arabian Sea

Westward moving eddies were evident in the Gulf of Aden during November–May (Figures 5.1–5.3) and our analysis showed them to be associated with westward propagating Rossby waves. Westward propagating Rossby waves in the Arabian Sea have also been noted in earlier studies. The Rossby waves in these studies were produced either by radiation from the west coast of India in association with poleward propagating coastal Kelvin waves [McCreary et al., 1993; Shankar and Shetye, 1997], or by the forcing due to Ekman pumping over the Arabian Sea (see, for example, [McCreary et al., 1993; Prasad and Ikeda, 2001; Brandt et al., 2002; Shankar et al., 2002]).

Prasad and Ikeda [2001] noticed an anticyclonic eddy in the vicinity of the gulf and attributed its existence to the arrival of Rossby waves from the interior Arabian Sea, speculating on the southern Arabian Sea high (situated at 5° N between $55\text{--}65^{\circ}$ E) as the possible source. They did not see the possibility of Rossby waves from the west coast of India reaching the gulf because of the Lakshadweep High (LH), a manifestation of Rossby waves radiated by poleward propagating Kelvin waves [Shankar and Shetye, 1997] in early winter, weakens in March and propagates in a northwestward direction before weakening further and breaking into smaller eddies along the path across the Arabian Sea. Brandt et al. [2002] also felt that the Rossby waves radiated from the LH would not reach the western boundary because those waves would gradually decay during their propagation. Kindle and Arnone [2001], however, did not discount the possibility of remnants of Rossby waves radiating from the west coast of India (specifically the LH) reaching the western boundary of the northern Arabian Sea; the process simulations of Shankar et al. [2002] also support the hypothesis that westward propagating Rossby waves from the Indian west coast propagate all the way across the Arabian Sea. The westward propagations seen in Figure 5.5 confirm this hypothesis, but significant modifications do occur on the way around $52\text{--}60^{\circ}$ E.

Based on the results of wavelet analysis, we conclude that (i) the annual Rossby waves are significant all over the basin, but the annual Ekman pumping is significant only west of 60° E, (ii) the years 2001–2003 are an exception to the above at 55° E, where the annual wavelets were insignificant, and (iii) the intense high-frequency oscillations ($\sim 90\text{--}180$ days) in SLA correspond to the intense high-frequency ($\sim 100\text{--}180$ days) oscillations in Ekman pumping at $52\text{--}58^{\circ}$ E (Figure 5.9a, b). This suggests that the westward propagating waves with periods less than ~ 180 days were produced locally (west of 60° E), but with some contribution from the east too. This longitude band ($52\text{--}60^{\circ}$ E) also appears to be special for the low-frequency (annual) westward propagating Rossby waves because they developed a discontinuity at this location (Figure 5.5b). A complete analysis of what

is so special about this longitude band for the Rossby waves is beyond the scope of this study because we basically want to relate the westward propagating mesoscale eddies in the Gulf of Aden and their origin in the westward propagating Rossby waves in the Arabian Sea. Similarly, the effect of reflected shortwave Rossby waves from the western boundary in modulating the westward propagating Rossby waves or their contribution to the eddies in the region is beyond the scope of the study. Nevertheless, in the following section, we list out four possible reasons for this longitude band being so special.

5.4.2 Discontinuity in the low–frequency Rossby waves in the western Arabian Sea

The first possible cause for the collapse of low–frequency waves and the increase in high–frequency waves between 52° E and 60° E could be the higher wind stress in this region during the summer monsoon. The annual wavelets of Ekman pumping, associated with the annual cycle of the monsoon, are significant only west of 60° E (Figure 5.9b). This would force annual Rossby waves, which need not necessarily be in phase with the Rossby waves propagating from the east. Depending on the phase difference between the locally forced SLA response and the Rossby waves from the east, constructive/destructive interference will create a discontinuity [Wang et al., 2001] similar to that noted in Figures 5.5 a and b. Wang et al. [2001] noticed a similar discontinuity in the annual Rossby waves in the interior of the southern Indian Ocean; that discontinuity was caused by constructive/destructive interference between the locally forced response and the Rossby waves propagating from the east.

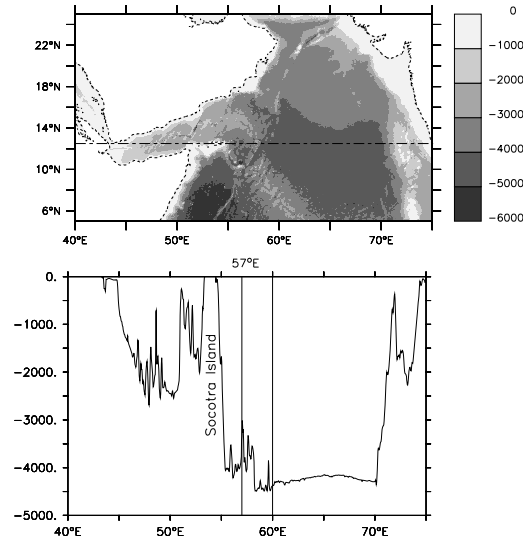
The high–frequency wavelets of Ekman pumping were energetic in this longitude band between 52° E and 58° E (especially between 52° E and 57° E) during 2001–2003, favouring the local generation of high–frequency Rossby waves (Figure 5.5a and c). The energetic Ekman pumping at 52 – 57° E during 2001–2003 also coincided with the strong discontinuity in the low–frequency waves (Figure 5.5b). Hence, it is likely that Ekman

pumping, both at low as well as at high-frequency, is involved in the generation of discontinuity in the low-frequency Rossby waves at these longitudes. The exact mechanism through which the high-frequency winds modulated the low-frequency Rossby waves is not clear from this analysis. Experiments with analytical or numerical models forced with different wind patterns is necessary to resolve this issue.

The second possibility is the bottom topography because the region is in the proximity of the, almost, meridionally oriented Carlsberg Ridge in this longitude band. Such topographic features are known to scatter the westward propagating Rossby waves, generated to their east, and change the phase (even up to 180°) across the ridge, thus causing them to break down [Barnier, 1988; Wang and Koblinsky, 1994]. A plot of bottom topography along 12.5° N based on ETOPO2v2 data ([National Geophysical Data Center, 2006], Figure 5.12) shows that the bottom rises by ~ 500 – 800 m west of 60° E (from ~ 4000 m to ~ 3500 – 3200 m) owing to the presence of the Carlsberg Ridge. It is unlikely, however, that the topographic scattering was effective in this case because the water column is still deep enough (> 3000 m) for the waves to propagate. This is more so because the propagation speed suggests the dominance of the first baroclinic mode Rossby waves. Also, it is not possible to invoke topography to explain the interannual variability seen in the vicinity of the discontinuity (Figure 5.5a and b) in the low-frequency waves. An exception is near 55° E, where the Socotra Island exists. It is possible that the presence of the island may affect the Rossby waves. The island could also affect the wind field and this possible cause of the high-frequency signal in the Ekman pumping (see Figure 5.9b) needs to be investigated; such an investigation is, however, beyond the scope of this work.

The third possible cause is the spatial structure of the thermocline, which can act, like bottom topography, to scatter the Rossby waves [Wang et al., 2001]. The thermocline, as indicated by the 18°C isotherm, along 12.5° N latitude first deepens towards the west from 75° E (~ 40 m) to 60° E (~ 175 m), and then shoals to ~ 60 m at 50° E (Figure 5.8d) in September, when the high frequency amplifications started west of \sim

Figure 5.12 The bottom topography of Arabian Sea based on ETOPO2v2 data [National Geophysical Data Center, 2006] depicting the northeast–south–southeast oriented Carlsberg Ridge. The depth along 12.5° N (the line marked in the upper panel) is shown in the lower panel.



60° E (Figure 5.5c) and the discontinuity started becoming apparent in the low–frequency waves (Figure 5.5b). Most notable is that the slope of the thermocline is steepest between 58° E and 60° E. The east–west thermocline structure in January, however, does not show appreciable variation from 75° E to 50° E.

The fourth possible cause is the anticyclonic Socotra Gyre that exists in the region during August–September (see Figure 36 in Schott and McCreary [2001]). The northeastern boundary of the Socotra Gyre lies in the longitude band 55–57° E. Simmons et al. [1988] stated that a pulse of high sea level propagates westward as a Rossby wave from the interior between 12° N and 14° N, arriving at 57° E in early September and causing intensification of the Socotra eddy. It is possible that the westward propagations are modified by the presence of the Socotra Gyre, which was shown by Shankar and Shetye [1997] to be the result of nonlinear dynamics.

In summary, we conclude that the westward propagating Rossby waves radiated from

the Indian west coast as well as the Rossby waves generated in the interior of the Arabian Sea ($52\text{--}60^\circ$ E) contribute to the cyclonic and anticyclonic eddies in the vicinity of the Gulf of Aden. The low-frequency signal (mainly annual signal) shows a discontinuity in the longitudinal band between 52° E and 60° E; its intensity and spatial extent demonstrate considerable interannual variability. Uplifting of the thermocline, local wind stress, and the presence of Socotra Gyre in the vicinity may all contribute to this discontinuity in the annual signal. The westward propagating high-frequency Rossby waves generated locally (west of 60° E) are also a source for westward propagating mesoscale eddies in the Gulf of Aden. They move into the gulf from the east, either directly or through the Socotra Passage. They survive and move westward within the gulf in spite of the frictional effect of the boundaries of the gulf.

The analysis suggests that the eddies entering the gulf from the Arabian Sea owe their existence to more than one mechanism. Local Ekman pumping is important during the summer monsoon (June–September). In May and during the latter half of the summer monsoon (late July to September) and the fall inter-monsoon (October), the dominant mechanism is the generation of eddies by the instabilities in the Somali Current and the large eddies associated with it (Great Whirl and Socotra eddy) [Fratantoni et al., 2006; Simmons et al., 1988]. During the winter monsoon (November–April), the dominant mechanism involves the westward propagating Rossby waves that are generated either in the Arabian Sea by Ekman pumping or along the west coast of India by poleward propagating Kelvin waves. Thus, the westward propagating Rossby waves from the Arabian Sea are more important for the circulation in the gulf over half the year. The multiple eddies and multiple processes that act in this western-boundary region make the case complicated. Numerical experiments with a primitive-equation model capable of separating the processes acting in the region are necessary for understanding details like the mechanisms that caused the discontinuity in the low-frequency waves and the enhancement in the high-frequency waves around 57° E.